analytical chemistry

Article

pubs.acs.org/ac

Sensitivity, Prediction Uncertainty, and Detection Limit for Artificial Neural Network Calibrations

Franco Allegrini and Alejandro C. Olivieri*

Departamento de Química Analítica, Facultad de Ciencias Bioquímicas y Farmacéuticas, Universidad Nacional de Rosario, Instituto de Química de Rosario (IQUIR-CONICET), Suipacha 531, Rosario S2002LRK, Argentina

Supporting Information

ABSTRACT: With the proliferation of multivariate calibration methods based on artificial neural networks, expressions for the estimation of figures of merit such as sensitivity, prediction uncertainty, and detection limit are urgently needed. This would bring nonlinear multivariate calibration methodologies to the same status as the linear counterparts in terms of comparability. Currently only the average prediction error or the ratio of performance to deviation for a test sample set is employed to characterize and promote neural network calibrations. It is clear that additional information is required. We report for the first time expressions that easily allow one to compute three relevant figures: (1) the sensitivity, which turns out to be sample-dependent, as expected, (2) the prediction uncertainty, and (3) the detection limit. The approach resembles that employed for linear multivariate calibration, i.e., partial least-squares regression, specifically adapted to neural network calibration scenarios. As usual, both simulated and real (near-infrared) spectral data sets serve to illustrate the proposal.

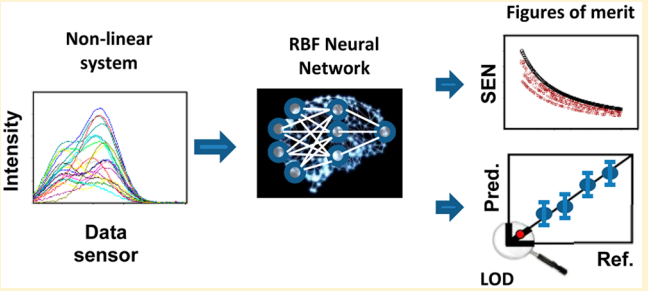

Multivariate calibration based on first-order data, e.g., near-infrared (NIR) spectra, is now ubiquitous in many analytical areas, with partial least-squares (PLS) regression being the most popular chemometric technique used for data processing.[1] Since PLS is based on a linear relationship between signal and concentration, alternative methodologies have been developed to handle nonlinearities, such as the use of polynomial functions[2] or kernel-PLS.[3] More powerful and flexible for nonlinear regression are artificial neural networks (ANN) which have been widely applied in spectroscopic calibration.[4,5] Recently, some pending issues in ANN calibration have been reviewed, such as (1) the presence of local minima, (2) the risk of overfitting, and (3) the need of very large sample sets for robust calibration.[6] The present report is devoted to solve an additional difficulty: the characterization of ANN methods with reliable figures of merit.

Many applications of ANN to analytical systems have been published,[7−10] including calibration-related problems in areas as diverse as fuels,[11,12] foodstuff,[13−15] pharmaceuticals,[16,17] and industrial products.[18,19] In the specific case of NIR applications, spectrometer manufacturers currently advertise ANN calibrations as simple, robust, and accurate.[20] However, usually the average prediction error or the ratio of performance to deviation (RPD)[21−23] for a test set of samples have been used to assess the accuracy in the case of nonlinear calibrations. No reports are available on the useful analytical figures of merit which characterize well-known models such as PLS.[24] An analogous development is urgently needed to put the statistical indicators at the same level of those for linear analytical models. This will allow one to report sensitivities, uncertainties in prediction, and detection capabilities for ANN calibrations.

Uncertainty propagation is a powerful tool to estimate analytical figures of merit, as has been shown in the past in the framework of linear calibration.[25] In the ANN field, it has been employed to select the most appropriate variables for modeling[26] and to discuss the sensitivity of the network parameters to the input data[27−29] but not the sensitivity of a particular ANN calibration methodology. In the present report, uncertainty propagation is exploited to define, for the first time, sensitivity, prediction uncertainty, and detection capabilities for multivariate calibration using neural networks based on radial basis functions (RBF).[30] The estimated parameters are illustrated with a set of simulated systems as well as with experimental NIR analytical calibrations. The obtained values are shown to be completely reasonable in view of the known properties of the studied analytical systems.

EXPERIMENTAL SECTION

Tecator NIR Data. These data consist of near-infrared absorbance spectra used to predict moisture, fat, and protein values of chopped meat. They were recorded on a Tecator Infratec Food and Feed Analyzer working in the wavelength range 850−1050 nm. Each sample contains finely chopped pure meat with different moisture, fat, and protein contents.[31] The

Received: May 12, 2016
Accepted: July 1, 2016
Published: July 1, 2016

DOI: 10.1021/acs.analchem.6b01857
Anal. Chem. 2016, 88, 7807−7812

set is usually employed for evaluating the performance of different multivariate calibration models, due to the presence of high nonlinearities in the signal-property relationships. The data were originally available at http://lib.stat.cmu.edu/datasets/tecator but cannot be presently accessed; they are available from the authors on request. They consist of 240 NIR spectra measured at 100 wavelengths, with the corresponding moisture, fat, and protein values. For multivariate calibration in the present context, the set was randomly divided in 170 spectra for calibration and 70 for test.

THEORY

Figures of Merit. One convenient way of defining the sensitivity in multivariate calibration is to add a small amount of independently and identically distributed (iid) noise to the multivariate signal of a generic test sample. This is conceptually used as a probe to explore the propagation of uncertainty from the test sample signal to the predicted analyte concentration. The parameter SEN is numerically defined as the ratio of input noise σ_x to output noise σ_y:

$$\mathrm{SEN} = \frac{\sigma_x}{\sigma_y} \tag{1}$$

In first-order PLS calibration, for example, the multivariate model yields a vector of regression coefficients b_{PLS}, which can be used for analyte prediction through

$$y = \mathbf{b}_{\mathrm{PLS}}^{\mathrm{T}}\mathbf{x} + \bar{y}_{\mathrm{cal}} \tag{2}$$

where $\mathbf{x}$ is the test sample spectrum and $\bar{y}_{\mathrm{cal}}$ is the mean calibration concentration (mean-centering is assumed). From eq 2, simple error propagation theory gives[24]

$$\mathrm{SEN} = \frac{1}{\|\mathbf{b}_{\mathrm{PLS}}\|} \tag{3}$$

where $\|\ \|$ indicates the norm of the vector.

Interestingly, there is a simple equivalent to eq 3 in ANN calibration of first-order data. A brief presentation is made here; for a more detailed discussion see the Supporting Information. The RBF network has A input neurons, N hidden neurons connected to the input neurons, and a single output neuron, which releases the predicted analyte concentration y. The transfer functions from the input to the hidden layer are Gaussian, while that to the output layer is linear, i.e., the output is given by

$$y = w_0 + \sum_{n=1}^{N} w_n \exp\left(-\sum_{a=1}^{A} \frac{[t(a) - c(n, a)]^2}{\sigma(a)^2}\right) = w_0 + \sum_{n=1}^{N} w_n f_n \tag{4}$$

where w_0 is a bias, w_n is the weight for the nth hidden neuron, $\sigma(a)$ is the standard deviation for each Gaussian function, and $c(n,a)$ is an element of the matrix $\mathbf{C}$ of Gaussian centers (size $N \times A$). The inputs are the sample scores estimated from principal component analysis (PCA), arranged into an $A \times 1$ vector $\mathbf{t}$, obtained by projection of the sample spectrum $\mathbf{x}$ ($J \times 1$) onto the space spanned by the PCA loadings ($\mathbf{P}$) considering A principal components:

$$\mathbf{t} = \mathbf{P}^{\mathrm{T}}\mathbf{x} \tag{5}$$

Uncertainty propagation proceeds by differentiation of eq 4, assuming that noise only affects the test sample:

$$\mathrm{d}y = \sum_{n=1}^{N} w_n \frac{\mathrm{d}f_n}{\mathrm{d}t(a)}\,\mathrm{d}t(a) \tag{6}$$

Taking into account eq 5, the following two expressions can be written:

$$\mathrm{d}t(a) = \mathbf{p}(a)^{\mathrm{T}}\,\mathrm{d}\mathbf{x} = \sum_{j=1}^{J} p(j, a)\,\mathrm{d}x(j) \tag{7}$$

$$\mathrm{d}y = \sum_{n=1}^{N} w_n \frac{\mathrm{d}f_n}{\mathrm{d}t(a)} \sum_{j=1}^{J} p(j, a)\,\mathrm{d}x(j) = \sum_{j=1}^{J} b_{\mathrm{ANN}}(j)\,\mathrm{d}x(j) = \mathbf{b}_{\mathrm{ANN}}^{\mathrm{T}}\,\mathrm{d}\mathbf{x} \tag{8}$$

with the individual elements of a sample dependent $\mathbf{b}_{\mathrm{ANN}}$ vector given by

$$b_{\mathrm{ANN}}(j) = \sum_{n=1}^{N} w_n \left[\sum_{a=1}^{A} \frac{\mathrm{d}f_n}{\mathrm{d}t(a)} p(j, a)\right] \tag{9}$$

Differentiating the transfer function f_n in eq 4 and replacing in eq 9:

$$b_{\mathrm{ANN}}(j) = -\sum_{n=1}^{N} w_n \left[\sum_{a=1}^{A} \frac{2[t(a) - c_n(a)]p(j, a)}{\sigma_n^2}\right] \exp\left(-\frac{\sum_{a=1}^{A}[t(a) - c_n(a)]^2}{\sigma_n^2}\right) \tag{10}$$

The variance in concentration is the expectation value of $\mathrm{d}\hat{y}^2$, i.e.,

$$E(\mathrm{d}\hat{y}^2) = E(\mathbf{b}_{\mathrm{ANN}}^{\mathrm{T}}\,\mathrm{d}\mathbf{x}\,\mathrm{d}\mathbf{x}^{\mathrm{T}}\mathbf{b}_{\mathrm{ANN}}) = \mathbf{b}_{\mathrm{ANN}}^{\mathrm{T}}\Sigma_x\mathbf{b}_{\mathrm{ANN}} \tag{11}$$

where Σ_x is the error variance-covariance matrix for the spectral data. In the event the noise structure is iid, Σ_x is diagonal with all nonzero elements equal to the spectral variance, and therefore

$$\sigma_y = \sigma_x\|\mathbf{b}_{\mathrm{ANN}}\| \tag{12}$$

where σ_y and σ_x are the uncertainties in predicted concentration and instrumental signal, respectively. From the latter equation, the sensitivity parameter SEN can be computed as the ratio of uncertainties (σ_x/σ_y):

$$\mathrm{SEN} = 1/\|\mathbf{b}_{\mathrm{ANN}}\| \tag{13}$$

In PLS, the vector of regression coefficients is unique for a given calibration data set and allows one to predict the analyte concentration through eq 2. In contrast, the neural network vector $\mathbf{b}_{\mathrm{ANN}}$ is not an analyte predictor and is specific for a given test sample, meaning that each specimen is characterized by a sensitivity value. ANN analytical protocols may thus report the mean, minimum and maximum sensitivity. This is in principle understandable, since the nonlinear relationship between signal and concentration implies that the slope of the latter relation depends on the analyte concentration and hence on the sample under scrutiny.

It may be noticed that a specific form of $\mathbf{b}_{\mathrm{ANN}}$ has been derived for an RBF network, which is usual in nonlinear spectral calibration. However, the developed scheme could in

DOI: 10.1021/acs.analchem.6b01857
Anal. Chem. 2016, 88, 7807−7812

principle be adapted to other ANN types such as feed-forward multilayer networks, with the main requirement that the transfer functions be differentiable. Work is under way in this direction.

Prediction uncertainty proceeds according to the well-known three-term expression, which accounts for the propagation from the errors in test sample signals, calibration signals, and calibration concentrations:

$$\sigma_{\hat{y}}^2 = \mathbf{b}_{\mathrm{ANN}}^{\mathrm{T}} \Sigma_x \mathbf{b}_{\mathrm{ANN}} + h \mathbf{b}_{\mathrm{ANN}}^{\mathrm{T}} \Sigma_x \mathbf{b}_{\mathrm{ANN}} + h \sigma_{\mathrm{ycal}}^2 \quad (14)$$

where h is the sample leverage and Σ_x is the calibration error variance-covariance matrix, as detailed in ref 32. The leverages can be calculated in a manner which is analogous to PCR or PLS models, from the design vector for a sample ($\mathbf{d}$) and the calibration design matrix ($\mathbf{D}$):

$$h = \mathbf{d}^{\mathrm{T}} (\mathbf{D}^{\mathrm{T}} \mathbf{D})^{-1} \mathbf{d} \quad (15)$$

where the elements of $\mathbf{d}$ for each sample are given by f_n, while $\mathbf{D}$ is defined by the design vectors for the calibration samples.

Equation 14 applies to a general noise structure. However, in the event the instrumental noise is iid, a much simpler expression is obtained:

$$\sigma_{\hat{y}}^2 = \sigma_x^2 \, \mathrm{SEN}^{-2} + h \sigma_x^2 \, \mathrm{SEN}^{-2} + h \sigma_{\mathrm{ycal}}^2 \quad (16)$$

where σ_x is the (constant) uncertainty in instrumental noise.

Finally, the limit of detection (LOD) can be given by a generalization of the already developed expressions for PLS regression.[33] For iid noise, the minimum and maximum LOD values are

$$\mathrm{LOD}_{\mathrm{min}} = 3.3(\sigma_x^2 \, \mathrm{SEN}_0^{-2} + h_{0\mathrm{min}} \sigma_x^2 \, \mathrm{SEN}_0^{-2} + h_{0\mathrm{min}} \sigma_{\mathrm{ycal}}^2) \quad (17)$$

$$\mathrm{LOD}_{\mathrm{max}} = 3.3(\sigma_x^2 \, \mathrm{SEN}_0^{-2} + h_{0\mathrm{max}} \sigma_x^2 \, \mathrm{SEN}_0^{-2} + h_{0\mathrm{max}} \sigma_{\mathrm{ycal}}^2) \quad (18)$$

where SEN_0 is the sensitivity, and $h_{0\mathrm{min}}$ and $h_{0\mathrm{max}}$ are the minimum and maximum leverage for a blank sample, respectively. The latter two values are estimated as described in ref 33 and represent the minimum and maximum leverages for the calibration set of samples, once they are extrapolated to the plane of zero analyte concentration. Details on these latter parameters can be found in the Supporting Information.

Simulations. Three simulated nonlinear systems were produced. In each of them, calibration models were built having three sample components and considering eight different degrees of spectral overlap and three signal noise levels. The components were present at random concentrations taken from the range 0−1 units in 100 calibration samples and from the range 0.2−0.8 in 50 test samples. Unit-concentration spectra of the components are shown in Figure 1, along with four selected degrees of overlap in the working range of 200 wavelengths.

The following relationships between signal and analyte concentration were considered: (1) quadratic, (2) sigmoidal, and (3) logarithmic. The specific expressions employed to generate the component signals were, respectively,

$$\mathbf{x}_n = 2\mathbf{s}_n y_n^2 \quad (19)$$

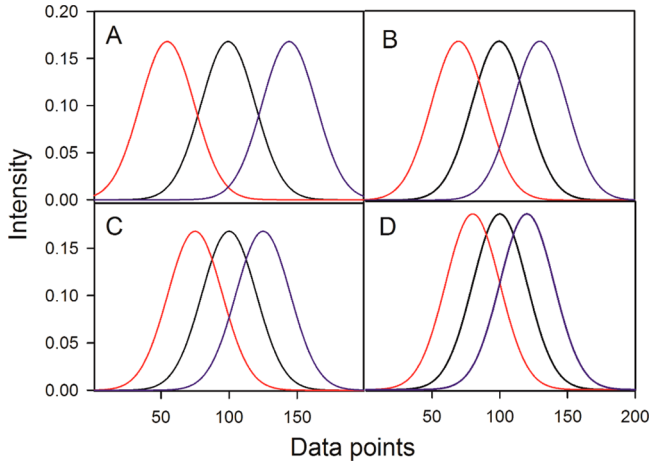

Figure 1. Pure component spectra for simulation. The panels show four selected overlapping situations of the eight studied ones, leading to the following four selectivity values for analyte 1: (A) 0.92, (B) 0.64, (C) 0.49, and (D) 0.34.

$$\mathbf{x}_n = \frac{2\mathbf{s}_n}{1 + \exp[-5(y_n - 0.5)]} \quad (20)$$

$$\mathbf{x}_n = -\mathbf{s}_n \ln(y_n) \quad (21)$$

In eqs 19−21, $\mathbf{x}_n$ is the sample signal for component n, $\mathbf{s}_n$ the signal for the pure component n, and y_n the component concentration. The selectivity for component 1 in each system is computed as $\|(\mathbf{I} - [\mathbf{s}_2|\mathbf{s}_3]\,[\mathbf{s}_2|\mathbf{s}_3]^{+})\,\mathbf{s}_1\|$, where $[\mathbf{s}_2|\mathbf{s}_3]$ is a two-column matrix built with $\mathbf{s}_2$ and $\mathbf{s}_3$, $\mathbf{I}$ is a unit matrix and the superscript "+" indicates pseudoinverse. Calibration ($\mathbf{x}_{\mathrm{cal}}$) and test ($\mathbf{x}_{\mathrm{test}}$) signals for each sample were computed by summing the individual $\mathbf{x}_n$ signals for each pure component according to the corresponding system.

In sum, a total of 14 400 different systems were produced, including 50 test samples, 8 degrees of spectral overlapping, 3 noise levels, 3 different noise structures (iid, correlated pink and proportional noise), and 4 different noise additions: (1) to test sample signals ($\mathbf{x}_{\mathrm{test}}$), (2) to calibration signals ($\mathbf{x}_{\mathrm{cal}}$), (3) to calibration concentrations (y_n), and (4) to all signals ($\mathbf{x}_{\mathrm{cal}}$ and $\mathbf{x}_{\mathrm{test}}$) and concentrations ($y_n$). Noise levels in concentration and signals were combined to create three types of systems, including low, middle, and high noise levels. The standard deviations in the calibration concentrations were set to 0.1% of the mean calibration concentration for low noise, 0.15% for intermediate noise, and 0.2% for high noise. Corresponding three levels of Gaussian iid noise and correlated pink noise were added in such a way that the signal standard deviation were 1%, 2.5%, and 4% of the mean spectral intensity value for the calibration samples. Finally, proportional noise was added with a proportionality factor of 0.01, 0.02, and 0.03 with respect to the signal at each sensor.

Calibration and prediction proceeded, in each case, by training ANNs of the RBF type according to the procedure described by Orr.[34,35] The input data to the ANN are not the raw signals but the scores obtained after principal component analysis (PCA) of the calibration data matrices. The number of hidden neurons was tuned by forward selection, with all transfer functions of the Gaussian type. To minimize overfitting during the training phase, generalized cross-validation was chosen as the model selection criterion, as suggested by Orr.[34] See the Supporting Information for further details.

DOI: 10.1021/acs.analchem.6b01857
Anal. Chem. 2016, 88, 7807−7812

Software. All simulations were carried out using MATLAB.[36] The Supporting Information provides an Appendix with two short MATLAB codes, which can be used to estimate the figures of merit in a typical RBF neural network calibration as the one presently discussed.

RESULTS AND DISCUSSION

Simulated Systems. After the individual ANNs were suitably trained, the $\mathbf{b}_{ANN}$ vector of eq 10 was computed for all the calibration samples, yielding the corresponding analyte sensitivities in the calibration set. The results are graphically summarized in the plots shown in Figure 2 in the case of iid addition. In the latter figures, the solid lines represent the sensitivity for the pure analyte as a function of its concentration, derived directly from the defining expressions (eqs 19−21). For clarity, four cases were selected from the eight different degrees of spectral overlap, namely, those leading to the lowest selectivities to analyte 1.

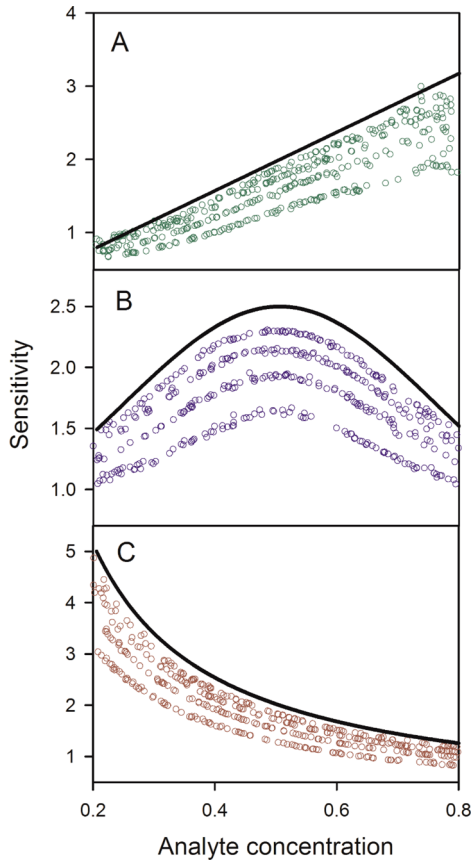

Figure 2. Theoretical sensitivity as a function of analyte concentration for selected simulated systems in the case of iid noise addition: (A) quadratic, (B) sigmoidal, and (c) logarithmic. In all cases, the solid line corresponds to the sensitivity for the pure analyte 1, and the circles to analyte 1 in three-component systems with increasing degree of spectral overlap. The sensitivity decreases in the direction of increasing spectral overlap.

For a system composed of analyte 1 as the only sample component, it is easy to see that the sensitivity will vary with the concentration because of the nonlinear nature of the signal-concentration relationship described by eqs 19−21. For example, in a quadratic system described by eq 19, the sensitivity increases linearly with analyte concentration, because the derivative of a second-degree polynomial is a linear function. In multicomponent systems, on the other hand, it is natural to expect that the sensitivities toward analyte 1 will not only change with its concentration but also with the degree of spectral overlap with additional sample components.

Figure 2 shows that the sensitivities closely follow the expected shapes of the SEN function for the pure analyte (solid lines). Interestingly, the values of SEN appear to be only dependent on the concentration of the analyte of interest, even when the latter is mixed with two additional components. Moreover, the values of SEN are smaller than the pure analyte sensitivity and decrease with increasing degree of spectral overlap. Overall, in all three studied systems, the behavior of the neural network sensitivity is consistent with the theoretical expectations.

The average, minimum and maximum values of SEN for each calibration set are collected in Table 1. All values are lower than the corresponding minimum and maximum values of slope of total signal vs concentration, computed for the pure analyte of interest. The latter are, from eqs 19−21, 0.8 and 3.6 for the quadratic system, 1.5 and 2.5 for the sigmoidal one, and 1.25 and 5 for the logarithmic. Furthermore, a reasonable trend to lower sensitivities is observed on increasing the spectral overlap, measured by the classical selectivity parameter among component spectra. Table 1 also reports the minimum and maximum limits of detection, computed with the aid of eqs 17 and (18. The reported values follow the same trend observed for the sensitivities, i.e., detection limits increase when the degree of spectral overlapping increases. Similar results to those shown in Figure 2 and Table 1 were obtained for the remaining simulated systems, i.e., for other overlapping degrees, levels,

Table 1. Sensitivities and Detection Limits for Analyte 1 in Selected Simulated Systems[a]

selectivity for analyte 1[b]	0.92	0.64	0.49	0.34
	Quadratic System			
SEN_{min}	0.8	0.7	0.5	0.4
SEN_{max}	3.2	2.3	1.6	1.4
⟨SEN⟩	1.9	1.3	1.0	0.7
LOD_{min}	0.004	0.005	0.007	0.009
LOD_{max}	0.006	0.007	0.009	0.01
	Sigmoidal System			
SEN_{min}	1.4	1.1	0.7	0.5
SEN_{max}	2.3	1.7	1.3	0.8
⟨SEN⟩	1.9	1.4	1.1	0.7
LOD_{min}	0.002	0.003	0.004	0.006
LOD_{max}	0.003	0.004	0.006	0.008
	Logarithmic System			
SEN_{min}	1.2	0.8	0.6	0.4
SEN_{max}	4.7	3.4	2.8	1.6
⟨SEN⟩	2.1	1.5	1.2	0.8
LOD_{min}	0.0008	0.001	0.001	0.002
LOD_{max}	0.001	0.002	0.002	0.003

[a] SEN_{min}, SEN_{max}, and ⟨SEN⟩ represent the minimum, maximum, and average sensitivity across the test sample set. LOD_{min} and LOD_{max} are the minimum and maximum detection limits. The results correspond to selected degrees of spectral overlap, in the case of addition of iid noise and for the lowest noise level. [b] Computed as described in the Simulations section.

DOI: 10.1021/acs.analchem.6b01857
Anal. Chem. 2016, 88, 7807−7812

and types of added noise. It is important to note that good agreement has been found between the prediction uncertainties estimated by noise addition and the values furnished by eq 14, as can be confirmed in Figures S1–S3 of the Supporting Information.

There is an interesting aspect of the set of $\mathbf{b}_{ANN}$ vectors. Figure S4 of the Supporting Information compares the range spanned by all calibration $\mathbf{b}_{ANN}$ vectors for the simulated systems with the vector of regression coefficients obtained by PLS calibration of the same data. The $\mathbf{b}_{PLS}$ vector, which is at the same time a predictor and SEN-estimator vector, rests within the boundaries of the range spanned by all $\mathbf{b}_{ANN}$ vectors, which are only SEN-estimators but not predictors. When PLS is applied to a nonlinear system, the regression vector tries to compensate for deviations of linearity with additional latent variables. One may thus expect the single $\mathbf{b}_{PLS}$ vector to be a sort of average of all the possible $\mathbf{b}_{ANN}$ vectors for a nonlinear system.

Experimental System. Regarding the determination of fat, moisture, and protein in chopped meat samples using NIR spectroscopy (Tecator data set); details on the composition of the data set can be found in Table 2. Individual PLS models (for comparison purposes) and RBF neural networks were trained for each parameter. Table 2 shows the PLS figures of merit estimated for the optimum number of latent variables, established by leave-one-out cross-validation. Also shown are the network architectures: the number of input neurons was estimated as the number of principal components (PCs) needed to explain at least 99% of the variance of the calibration data, whereas the number of hidden neurons was tuned by forward selection, as detailed for the simulated data sets. The suitability of the selected number of input neurons can be appreciated in a plot of the average prediction error as a function of the number of PCs, noting that the error stabilizes at the selected number of PCs for all three target properties (see Figure S5 of the Supporting Information).

The results in terms of predictive ability are similar to those recently reported using a variety of neural networks, and are significantly better than those reached with PLS calibration (Table 2).[6] This is confirmed by the plot of predicted vs nominal sample properties, shown in Figure S6 of the Supporting Information, both for PLS and the present ANN approach. The corresponding analytical figures of merit are shown in Table 2. ANN sensitivities were calculated from the $\mathbf{b}_{ANN}$ vectors for each sample in each system, as illustrated in Figure 3. Table 2 confirms better sensitivity for ANN in comparison with PLS, in line with the RMSEP results, although the difference is less marked in the case of protein determination.

Table 2. Characteristics of the Experimental Data Set and Analytical Figures of Merit for PLS and ANN Calibrations[a]

	fat/%	moisture/%	protein/%
no. of calibration samples		170	
no. of test samples		70	
property range	32.8–76.6	0.9–58.5	8.8–23.2
mean calibration value	63.0	18.3	17.7
calibration standard deviation	10.7	13.9	3.3
calibration minimum value	32.8	0.9	8.8
calibration maximum value	76.6	58.5	23.2
mean test value	62.5	18.9	18.0
test standard deviation	11.8	15.5	3.9
test minimum value	34.1	0.9	9.0
test maximum value	76.6	56.1	23.2
σ_{ycal}	1.06	0.71	0.78
σ_x		6.4×10^{-5}	
		PLS Calibration	
no. of latent variables[b]	11	11	10
RMSEP	2.4	2.8	0.76
REP%	3.8	15.3	4.3
SEN	0.00042	0.00041	0.0011
LOD_{min}	3.8	1.6	1.3
LOD_{max}	6.3	5.3	1.8
		ANN Calibration	
ANN architecture	15-54-1	15-46-1	15-47-1
RMSEP	0.71	0.59	0.64
REP%	1.1	3.2	3.6
SEN_{min}	0.0016	0.0034	0.0016
SEN_{max}	0.0041	0.0051	0.0035
⟨SEN⟩	0.0021	0.0040	0.0018
LOD_{min}	1.6	0.3	1.1
LOD_{max}	3.8	2.3	2.7

[a]Network architecture given as input-hidden-output number of neurons; RMSEP, root-mean-square error of prediction; REP%, relative error of prediction with respect to the mean calibration property value. [b]Estimated by leave-one-out cross-validation.

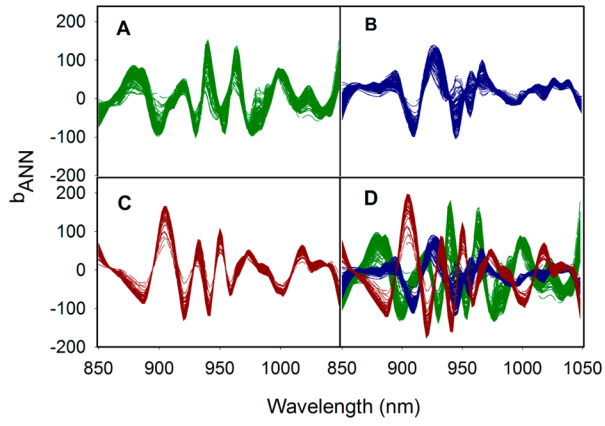

Figure 3. Sensitivity coefficients for artificial neural network in (A) fat data set, (B) moisture data set, (C) protein data set, and (D) fat, moisture, and protein together.

To estimate the range of detection limits, the uncertainty in instrumental signals (σ_y) was estimated as the spectral residue of the PCA decomposition of the calibration data matrix. The value of the uncertainty in concentration (σ_{ycal}) may be known from previous laboratory experience or from the uncertainty in the reference analytical method. In the present case, since this information was not available, a cross validation average error was calculated for each property using the calibration set and employed as an approximate estimator. With the latter values, minimum and maximum limits of detection can be estimated, as reported in Table 2 for all three calibrated parameters. Following the same trend as the average prediction error and sensitivities, the detection limits are in general smaller for ANN calibration than for the PLS models (they are comparable in the case of protein determination). The LOD results appear to be reasonable in light of the average prediction errors for the test sample set, i.e., LOD_{min} values are on the order of the RMSEP for each analyte (Table 2). In any case, the extrapolation to

DOI: 10.1021/acs.analchem.6b01857
Anal. Chem. 2016, 88, 7807–7812

zero analyte concentration implied by the LOD expressions (eqs 17 and 18) is safer in the case of the moisture determination, because low levels of the target property are available in the calibration set (Table 2).

CONCLUSIONS

The current expansion and widespread use of artificial neural networks to develop first order analytical calibrations demands the development of reliable estimators of the figures of merit that are normally used to characterize these calibrations. In response to this need, a full battery of estimators is presented for sensitivity, sample dependent prediction error, and limit of detection. They are described and validated over simulated and experimental data sets processed with radial basis function neural networks. The developed expressions follow previous developments in the context of other well-known analytical calibration models and represent a link between linear and nonlinear calibration worlds in terms of model validation. As a consequence, the estimators provide analytical chemists with additional tools to perform reliable comparisons between first-order models as well as a deeper insight into neural network mechanisms. Finally, the proposal sets a conceptual basis for extending the estimators to other popular strategies dealing with nonlinear data, such as back-propagation neural networks and support vector machines.

ASSOCIATED CONTENT

Supporting Information

The Supporting Information is available free of charge on the ACS Publications website at DOI: 10.1021/acs.analchem.6b01857.

Monte Carlo simulations, figures of merit, plots of $\mathbf{b}_{ANN}$ vectors, prediction plots for PLS and ANN, appendix of two short MATLAB codes, and references (PDF)

AUTHOR INFORMATION

Corresponding Author

*Fax: +54-341-4372704. E-mail: olivieri@iquir-conicet.gov.ar.

Notes

The authors declare no competing financial interest.

ACKNOWLEDGMENTS

Universidad Nacional de Rosario, CONICET (Consejo Nacional de Investigaciones Científicas y Técnicas, Project No. PIP 0163), ANPCyT (Agencia Nacional de Promoción Científica y Tecnológica, Project No. PICT-2013-0136) are gratefully acknowledged for financial support. F.A. thanks CONICET for a postdoctoral fellowship.

REFERENCES

(1) Haaland, D. M.; Thomas, E. V. *Anal. Chem.* **1988**, *60*, 1193−1202.
(2) Wold, S.; Kettaneh-Wold, N.; Skagerberg, B. *Chemom. Intell. Lab. Syst.* **1989**, *7*, 53−65.
(3) Park, J. I.; Liu, L.; Ye, X. P.; Jeong, M. K.; Jeong, Y. *Expert Syst. Appl.* **2012**, *39*, 1555−1564.
(4) Hanrahan, G. *Anal. Chem.* **2010**, *82*, 4307−4313.
(5) Jalali-Heravi, M. Neural Networks in Analytical Chemistry. In *Artificial Neural Networks*; Methods in Molecular Biology, Vol. *458*; Humana Press: Totowa, NJ, 2008; pp 81−121.
(6) Ni, W.; Nørgaard, L.; Mørup, M. *Anal. Chim. Acta* **2014**, *813*, 1−14.
(7) Mikami, D.; Ohki, T.; Yamaji, K.; Ishihara, S.; Citterio, D.; Hagiwara, M.; Suzuki, K. *Anal. Chem.* **2004**, *76*, 5726−5733.
(8) García-Reiriz, A.; Damiani, P. C.; Olivieri, A. C.; Cañada-Cañada, F.; Muñoz de la Peña, A. *Anal. Chem.* **2008**, *80*, 7248−7256.
(9) Webster, G. T.; de Villiers, K. A.; Egan, T. J.; Deed, S.; Tilley, L.; Tobin, M. J.; Bambery, K. R.; McNaughton, D.; Wood, B. R. *Anal. Chem.* **2009**, *81*, 2516−2524.
(10) Miller, T. H.; Musenga, A.; Cowan, D. A.; Barron, L. P. *Anal. Chem.* **2013**, *85*, 10330−10337.
(11) Stratiev, D.; Marinov, I.; Dinkov, R.; Shishkova, I.; Velkov, I.; Sharafutdinov, I.; Nenov, S.; Tsvetkov, T.; Sotirov, S.; Mitkova, M.; Rudnev, N. *Energy Fuels* **2015**, *29*, 1520−1533.
(12) Balabin, R. M.; Safieva, R. Z.; Lomakina, E. I. *Fuel* **2011**, *90*, 2007−2015.
(13) Dong, W.; Ni, Y.; Kokot, S. *J. Agric. Food Chem.* **2013**, *61*, 540−546.
(14) Bessant, C.; Saini, S. *Anal. Chem.* **1999**, *71*, 2806−2813.
(15) Marini, F. *Anal. Chim. Acta* **2009**, *635*, 121−131.
(16) Wang, B.; Liu, G.; Dou, Y.; Liang, L.; Zhang, H.; Ren, Y. *J. Pharm. Biomed. Anal.* **2009**, *50*, 158−163.
(17) Yao, H. C.; Sun, M.; Yang, X. F.; Zhang, Z. Z.; Li, H. *J. Pharm. Anal.* **2011**, *1*, 32−38.
(18) Despagne, F.; Massart, D. L.; Chabot, P. *Anal. Chem.* **2000**, *72*, 1657−1665.
(19) Rounaghi, G.; Mohammad, R.; Kakhki, Z.; Heidari, T. *Ind. Eng. Chem. Res.* **2011**, *50*, 11375−11381.
(20) Anderson, S. *J. AOAC Int.* **2007**, *90*, 1073−1083.
(21) Farifteh, J.; Van Der Meer, F.; Atzberger, C.; Carranza, E. J. M. *Remote Sens. Environ.* **2007**, *110*, 59−78.
(22) Mouazen, A. M.; Kuang, B.; De Baerdemaeker, J.; Ramon, H. *Geoderma* **2010**, *158*, 23−31.
(23) Viscarra Rossel, R. A.; Behrens, T. *Geoderma* **2010**, *158*, 46−54.
(24) Olivieri, A. C.; Faber, N. M.; Ferré, J.; Boqué, R.; Kalivas, J. H.; Mark, H. *Pure Appl. Chem.* **2006**, *78*, 633−661.
(25) Olivieri, A. C. *Chem. Rev.* **2014**, *114*, 5358−5378.
(26) Despagne, F.; Massart, D. L. *Chemom. Intell. Lab. Syst.* **1998**, *40*, 145−163.
(27) Derks, E. P. P. A.; Sánchez Pastor, M. S.; Buydens, L. M. C. *Chemom. Intell. Lab. Syst.* **1995**, *28*, 49−60.
(28) Faber, K.; Kowalski, B. R. *Chemom. Intell. Lab. Syst.* **1996**, *34*, 293−297.
(29) Derks, E. P. P. A.; Sánchez Pastor, M. S.; Buydens, L. M. C. *Chemom. Intell. Lab. Syst.* **1996**, *34*, 299−301.
(30) Mark, J.; Orr, L. *Introduction to Radial Basis Function Networks: Recent Advances in Radial Basis Function Networks*; Centre for Cognitive Science, University of Edinburgh: Edinburgh, Scotland, 1996; pp 1−67.
(31) Borggaard, C.; Thodberg, H. H. *Anal. Chem.* **1992**, *64*, 545−551.
(32) Allegrini, F.; Wentzell, P. D.; Olivieri, A. C. *Anal. Chim. Acta* **2016**, *903*, 51−60.
(33) Allegrini, F. A.; Olivieri, A. C. *Anal. Chem.* **2014**, *86*, 7858−7866.
(34) Orr, M. J. L. *Matlab Functions for Radial Basis Function Networks*, Technical report, Institute for Adaptive and Neural Computation, Division of Informatics, Edinburgh University: Edinburgh, Scotland, 1999.
(35) Orr, M. J. L. *Neural Comp.* **1995**, *7*, 606−623.
(36) *MATLAB*, version R2012a; The Mathwork: Natick, MA, 2012.

DOI: 10.1021/acs.analchem.6b01857
Anal. Chem. 2016, 88, 7807−7812